Digital micromirror device-based common-path quantitative phase imaging

Citation: Zheng, Cheng, Renjie Zhou, Cuifang Kuang, Guangyuan Zhao, Zahid Yaqoob, and Peter T. C. So. "Digital Micromirror Device-Based Common-Path Quantitative Phase Imaging." Optics Letters 42, no. 7 (March 31, 2017): 1448. © 2017 Optical Society of America.

As Published: http://dx.doi.org/10.1364/OL.42.001448

Publisher: The Optical Society

Persistent URL: http://hdl.handle.net/1721.1/120010

Version: Author's final manuscript: final author's manuscript post peer review, without publisher's formatting or copy editing

HHS Public Access

Author manuscript

Opt Lett. Author manuscript; available in PMC 2018 April 01.

Published in final edited form as:

Opt Lett. 2017 April 01; 42(7): 1448–1451.

Digital micromirror device-based common-path quantitative phase imaging

Cheng Zheng[1,†], **Renjie Zhou**[2,*,†], **Cuifang Kuang**[1], **Guangyuan Zhao**[1], **Zahid Yaqoob**[2,5], and **Peter T. C. So**[2,3,4]

[1]State Key Laboratory of Modern Optical Instrumentation, College of Optical Science and Engineering, Zhejiang University, Hangzhou 310027, China

[2]Laser Biomedical Research Center, G. R. Harrison Spectroscopy Laboratory, Massachusetts Institute of Technology, Cambridge, Massachusetts 02139, USA

[3]Department of Mechanical Engineering, Massachusetts Institute of Technology, Cambridge, Massachusetts 02139, USA

[4]Department of Biological Engineering, Massachusetts Institute of Technology, Cambridge, Massachusetts 02139, USA

Abstract

We propose a novel common-path quantitative phase imaging (QPI) method based on a digital micromirror device (DMD). The DMD is placed in a plane conjugate to the objective back-aperture plane for the purpose of generating two plane waves that illuminate the sample. A pinhole is used in the detection arm to filter one of the beams after sample to create a reference beam. Additionally, a transmission-type liquid crystal device, placed at the objective back-aperture plane, eliminates the specular reflection noise arising from all the “off” state DMD micromirrors, which is common in all DMD-based illuminations. We have demonstrated high sensitivity QPI, which has a measured spatial and temporal noise of 4.92 nm and 2.16 nm, respectively. Experiments with calibrated polystyrene beads illustrate the desired phase measurement accuracy. In addition, we have measured the dynamic height maps of red blood cell membrane fluctuations, showing the efficacy of the proposed system for live cell imaging. Most importantly, the DMD grants the system convenience in varying the interference fringe period on the camera to easily satisfy the pixel sampling conditions. This feature also alleviates the pinhole alignment complexity. We envision that the proposed DMD-based common-path QPI system will allow for system miniaturization and automation for a broader adaption.

Ever since the development of phase contrast (PC) microscopy, the phase of electromagnetic fields has been considered an important contrast mechanism for visualizing structural features of the specimen under study [1]. Nomarski subsequently invented differential-

*Corresponding author: renji@mit.edu.

[5]zyaqoob@mit.edu

†These authors contributed equally to this work.

OCIS codes: (170.0110) Imaging systems; (120.3180) Interferometry; (120.5050) Phase measurement; (110.0180) Microscopy; (120.0120) Instrumentation, measurement, and metrology.

interference contrast (DIC) microscopy that relies on one-dimensional phase gradient image contrast enhancement [2]. Although PC and DIC are among the most popular techniques for biological imaging, neither allows for quantitative measurement of the sample-induced optical phase. In contrast, quantitative phase imaging (QPI) methods precisely measure the relative phase shifts associated with sample thickness and refractive index distribution, thus providing label-free image contrast without any sample preparation [3–9]. Phase measurements were well known to be affected by the mechanical vibrations and air fluctuations, which has motivated the development of common-path interferometry, thereby achieving shot-noise limited detection with phase sensitivity better than a few milliradians [9–15]. Over the last decade, QPI techniques have become an important modality for quantifying cell dynamics [3,9,10,16–20] and material metrology [19,21].

In this Letter, we propose a new common-path QPI system based on a DMD. Our system is similar to a diffraction phase microscope (DPM) [9] in the way that it also uses a pinhole to generate a reference beam, but it does not require a physical diffraction grating to create two image copies. Our system uses an active DMD to control the illumination beam that offers two key advantages: flexibility in varying the interference fringe period on the camera to satisfy the pixel sampling conditions, and a simplification of the pinhole alignment process as in DPM. Another important innovation is that we have effectively increased the contrast ratio of the DMD by 400 through adding a transmission-type liquid crystal device (LCD) for additional filtering, which removes the specular reflection background noise from the DMD. The proposed QPI system also features an off-axis interferometry configuration that allows for high-speed phase imaging with speed only limited by the camera; thus, it is ideal for measuring sample dynamics.

We first briefly introduce the working principle of our DMD-based QPI system. The DMD is a micro-electromechanical system (MEMS) device consisting of more than several hundred thousand tiny switchable micromirrors. Each micromirror has two stable states (i.e., surface normal at either +12 deg or −12 deg) that determine the direction of the deflected light. When a micromirror is set at +12 deg, it is referred to as “on” state. Correspondingly, at −12 deg, the micromirror is referred to as “off” state. This characteristic makes DMD a binary amplitude spatial light modulator (SLM).

Traditionally, DMDs are used in a conjugate image plane as an adjustable dynamic aperture [22–25]. In our setup, as illustrated in Fig. 1, we place the DMD in a conjugate Fourier plane to engineer the illumination beam with controllable incident angles on the sample. A 532 nm laser is expanded and collimated to ensure uniform illumination onto the DMD (DLP3000 LightCrafter, Texas Instruments, pixel pitch 10.8 μm). Two macro pixels are opened on the DMD, one with 16 × 8 pixels and the other with 4 × 2 pixels, to first make two collimated waves on the sample and then on the camera. Relayed by a $4f$ system, the two point light sources are projected on a transmission LCD that is sandwiched between two cross-polarized linear polarizers, making the LCD an amplitude SLM. On the LCD, we also open two square windows, corresponding to the same DMD opening areas for an additional filtering of the residual specular reflection signal from the “off” state micromirrors. This feature improves the DMD contrast ratio by more than 2 orders of magnitude because the new contrast ratio is now the multiplication of the contrast ratios of both the LCD and the

DMD. The insertion of the LCD is crucial to remove the DMD residual noise signal, as illustrated in Fig. 2. Two filtered beams from the LCD pass through a 40 ×/1.3 oil immersion Zeiss objective (used as a condenser lens) and illuminate the sample. The corresponding transmitted beams are subsequently collected by an imaging objective lens of the same numerical aperture and form an interference fringe pattern at the imaging plane.

To create a reference beam, another 4*f* system is added in the detection arm, where in the Fourier plane, a pinhole is used to low-pass filter one of the beams. The pinhole has a 30-μm-diameter opening area, and the Fourier lens prior to the pinhole has a 50 mm focal length. The pinhole lateral position is aligned with the 16 × 8 macro pixel on the DMD plane. The reason for aligning pinhole with the larger macro pixel is that it will ensure a balanced power for better interference fringe contrast. The final interferogram is formed through an imaging lens and captured by a CMOS camera (DCC1545M, Thorlabs) on the image plane.

As briefly mentioned, the LCD overcomes the deficiency of DMD contrast ratio (DLP3000 LightCrafter has a contrast ratio of 685:1). Owing to the low contrast ratio of the DMD, the residual specular reflection from the “off” state micromirrors, which covers most of the whole DMD area, will converge at the sample plane as well as at the final image plane to form a bright spot as shown in Fig. 2(a). This bright spot washes out the fringe contrast and also generates additional unstable interference patterns. In Fig. 2(b), the Fourier plane image (modulus of the Fourier transform in log scale) clearly shows unexpected background noise at the first order, which will adversely influence the phase retrieval results. In Fig. 2(c), we show the corresponding phase image, where the phase retrieval fails at the bright spot area, and a slight modulation pattern is also observed. With the help of the LCD placed in the conjugate plane, we can further attenuate the residual signal arising from the “off” state micromirrors by another factor of 400 (the contrast ratio of this type of LCD has been measured and reported in Ref. [26]), thus achieving an overall contrast ratio of around 274,000:1. This combination (DMD plus LCD) successfully filters the entire DMD residual signal, such that the bright spot is completely removed, resulting in a significantly improved fringe contrast as shown in Fig. 2(d). Furthermore, the Fourier spectrum of the filtered interferogram [see Fig. 2(e)] displays a clean background. As expected, this has resulted in a better phase measurement in Fig. 2(f). We also quantified the noise improvement: the temporal noise is enhanced from 2.96 nm to 2.16 nm, while the spatial noise is enhanced from 5.87 nm to 4.92 nm (noise measurement procedure follows section 2.4 in [19]). The spatial noise of our system is comparable to the previously reported systems [19]. Although our system’s temporal noise is 2× higher, but under shot-noise limited detection, these noise values are expected by considering that our USB camera has an electron well depth of about 10,000, which is roughly 4× smaller than a normal scientific camera (in QPI, the temporal noise is inversely proportional to the square root of the electron well depth [15]).

The QPI capability of the system is tested by measuring calibrated samples. We suspend polystyrene beads ($n = 1.59$, Thermo Scientific) in index-matching liquid ($n = 1.56$) for observation. An interferogram of a 10-μm-diameter bead, indicated by a red dashed square, is shown in Fig. 3(a). The spatially resolved quantitative phase map, $\phi(x, y)$, associated with

the interferogram is retrieved using the Fourier transform method [19] and converted into the height map, $h(x, y)$, through using the relation

$$h(x,y)=\frac{\phi(x,y)\lambda}{2\pi\Delta n}, \quad (1)$$

where λ = 532 nm is the wavelength of the laser source in vacuum and Δn = 0.03 is the refractive index contrast between the bead and the surrounding medium. The height map presented in Fig. 3(b) shows a clean background, thanks to the additional LCD filtering. A height profile along the white dashed line across the center of the bead in Fig. 3(b) is also plotted in Fig. 3(c). The height of the bead was quantified as 9.4 μm, and its diameter is close to 10 μm. To demonstrate the system's ability in quantifying cellular structures, we image live human RBCs suspended in a phosphate-buffered saline (PBS) solution as shown in Fig. 3(d). Clear fringes with obvious bending can be observed in the RBC region. The particular RBC is an echinocyte with rough surface shape that deviates from the typical biconcave disk or discocyte shape. The shape change happened because the PBS solution was hypertonic for the RBCs; the higher osmotic pressure caused shrinkage of RBCs within the medium [27].

RBCs have simple structures with soft plasma membranes. Driven by thermal dynamics, the membrane of a RBC can fluctuate with a relatively large magnitude of around 100 nanometers [16,28]. Next, we use our system to quantify RBC membrane fluctuations by monitoring the height variation across the cell. About 200 consecutive interferograms of a discocyte were recorded at the frame rate of 25 frames per second (fps). Figures 4(a) and 4(b) show the interferogram and phase map for one of the frames. A time-lapse of the height map in a bird's-eye view is presented in Fig. 4(c), and the dynamic variation can be seen in Visualization 1. The membrane fluctuation is quantified by a standard deviation map of the height fluctuation, as shown in Fig. 4(d). From this image, we found that the magnitude of the fluctuation at the outer part of the cell is mostly around or less than 100 nm, which agrees with previous reports in [9,16]. The areas that have more than 100 nm height fluctuations might be due to lateral direction motions around the RBC edge.

One advantage of using DMD is that it grants the convenience of changing the spatial frequency, i.e., fringe period and orientation, of the interferograms. To do that, we first use the desired fringe period and orientation angle to calculate the spatial frequency magnitudes in x and y. Then, we convert the magnitude values into DMD pixel numbers, which are used to determine the center distance of the two macro pixel opening areas on the DMD. Finally, we display the corresponding DMD pattern. In Fig. 5, we experimentally verify this point by measuring the fringes of different orientations [Figs. 5(a)–5(c)] and frequencies [Figs. 5(d)–5(f)] by digitally changing the two macro square patterns on DMD. It should be noted that in the current results, we have observed variations in the fringe contrast and also noise-like patterns. We attribute this to the performance of the LCD, which has unexpected angle-dependent amplitude modulations. This issue can be potentially solved by using another DMD because it offers more stability (note: DMD operates in reflection mode, thus an

additional 4*f* system might be required). As another advantage, we have demonstrated that the DMD can facilitate the tedious manual pinhole alignment by digitally scanning the center position of the macro pixel that corresponds to the 30 μm physical pinhole, thus allowing for automatic pinhole position drift correction.

In summary, we have reported a DMD-based common-path QPI method to measure the morphology of microscopic structures with high precision and high speed. The DMD offers flexibility in varying the interference fringe period on the camera to satisfy the pixel sampling conditions as well as simplifying the pinhole alignment. Importantly, the implementation of an LCD has improved the phase measurement accuracy by eliminating the residual noise caused by the relatively low contrast ratio of a DMD. The digitally controllable property of DMD and LCD makes it easy in changing system designs, thus allowing for further software development and miniaturizing of the system footprint.

In the future, to take the advantage of fast illumination angle scanning of DMD, high-speed synthetic aperture imaging can be demonstrated without physically rotating the gratings as done in Ref. [29] or using galvanometer mirrors as in Ref. [30]. It should be pointed that although the LCD cannot refresh at high speed, we can turn on all the needed macro pixels on the same LCD pattern and keep it while the DMD is refreshing. One drawback of the Fourier space illumination is the low power efficiency. In our experiments, we used 50 mW laser power, which converts to about 20 μW power after the DMD and a few μW on the camera, which is enough for the camera to operate at 25 fps (note: 1 μW power is enough to fill up the well depth of the camera). Recently, we found that the power efficiency can be easily improved by writing Lee holograms on the DMD and placing it in the conjugate sample plane [31] (note that this illumination scheme will still require additional filtering of the undesired light diffraction orders). Although the illumination based on a DMD plus an LCD has reduced most of the spatial noise in our system, our phase images still have noises from multiple reflections due to the use of a highly coherent laser (the Verdi V18 laser that we use has over 10 m coherence length). This issue can be mitigated by using a relatively broad band light source (such as a mode-locked laser as used in [15] or a supercontinuum source) or averaging of multiple measurements under different sample illuminations (e.g., an electrically focus tunable lens has been used to modulate the sample illumination amplitude and phase in [32]).

Acknowledgments

Funding. National Basic Research Program of China (973 Program) (2015CB352003); National Natural Science Foundation of China (NSFC) (61335003, 61378051, 61427818); Natural Science Foundation of Zhejiang Province (LR16F050001); Fundamental Research Funds for the Central Universities (2016FZA5002); National Institutes of Health (NIH) (1R01HL121386-01A1, 9P41EB015871-26A1); BioSystems and Micromechanics Inter-Disciplinary Research program, Singapore-MIT Alliance for Research and Technology Centre (SMART); Open Foundation of the State Key Laboratory of Modern Optical Instrumentation; Hamamatsu Corp.

References

1. Zernike F. Physica. 1942; 9:974.
2. Nomarski, G. Interferential polarizing device for study of phase objects. US patent. 2,924,142 A. Feb 9. 1960
3. Popescu, G. Quantitative Phase Imaging of Cells and Tissues. McGraw-Hill; 2011.

4. Dunn GA, Zicha D, Fraylich PE. J Cell Sci. 1997; 110:3091. [PubMed: 9365279]
5. Cuche E, Marquet P, Depeursinge C. Appl Opt. 1999; 38:6994. [PubMed: 18324243]
6. Kemper B, von Bally G. Appl Opt. 2008; 47:A52. [PubMed: 18239699]
7. Popescu G, Deflores LP, Vaughan JC, Badizadegan K, Iwai H, Dasari RR, Feld MS. Opt Lett. 2004; 29:2503. [PubMed: 15584275]
8. Ikeda T, Popescu G, Dasari RR, Feld MS. Opt Lett. 2005; 30:1165. [PubMed: 15945142]
9. Popescu G, Ikeda T, Dasari RR, Feld MS. Opt Lett. 2006; 31:775. [PubMed: 16544620]
10. Wang Z, Millet L, Mir M, Ding H, Unarunotai S, Rogers J, Gillette MU, Popescu G. Opt Express. 2011; 19:1016. [PubMed: 21263640]
11. Shaked NT. Opt Lett. 2012; 37:2016. [PubMed: 22660106]
12. Hillman TR, Lue N, Sung Y, Dasari RR, Yaqoob Z. IEEE Photon Technol Lett. 2012; 24:1812.
13. Lee K, Park Y. Opt Lett. 2014; 39:3630. [PubMed: 24978554]
14. Mico V, Ferreira C, Zalevsky Z, García J. Opt Express. 2014; 22:14929. [PubMed: 24977587]
15. Hosseini P, Zhou R, Kim YH, Peres C, Diaspro A, Kuang CF, Yaqoob Z, So PTC. Opt Lett. 2016; 41:1656. [PubMed: 27192311]
16. Park Y, Best CA, Auth T, Gov NS, Safran SA, Popescu G, Suresh S, Feld MS. Proc Natl Acad Sci USA. 2010; 107:1289. [PubMed: 20080583]
17. Park Y, Best CA, Badizadegan K, Dasari RR, Feld MS, Kuriabova T, Henle ML, Levine AJ, Popescu G. Proc Natl Acad Sci USA. 2010; 107:6731. [PubMed: 20351261]
18. Mir M, Wang Z, Shen Z, Bednarz M, Bashir R, Golding I, Prasanth SG, Popescu G. Proc Natl Acad Sci USA. 2011; 108:13124. [PubMed: 21788503]
19. Bhaduri B, Edwards C, Pham H, Zhou R, Tan HN, Goddard LL, Popescu G. Adv Opt Photon. 2014; 6:57.
20. Bhaduri B, Pham H, Mir M, Popescu G. Opt Lett. 2012; 37:1094. [PubMed: 22446236]
21. Zhou R, Edwards C, Arbabi A, Popescu G, Goddard LL. Nano Lett. 2013; 13:3716. [PubMed: 23899129]
22. Liang M, Stehr RL, Krause AW. Opt Lett. 1997; 22:751. [PubMed: 18185650]
23. Chao, SH., Ren, TTH., Gales, SA., Holl, MR. IEEE/RAS-EMBS International Conference on Biomedical Robotics and Biomechatronics; IEEE; 2006. p. 977-981.
24. Zhang C, Huang PS, Chiang FP. Appl Opt. 2002; 41:5896. [PubMed: 12371547]
25. Dan D, Lei M, Yao B, Wang W, Winterhalder M, Zumbusch A, Qi Y, Xia L, Yan S, Yang Y. Sci Rep. 2013; 3:570.
26. Edwards C, Bhaduri B, Tan N, Griffin BG, Pham H, Kim T, Popescu G, Goddard LL. Opt Express. 2014; 22:5133. [PubMed: 24663853]
27. Sperelakis, N. Cell Physiology Source Book. 2. Academic; 1998.
28. Brochard F, Lennon JF. J Phys. 1975; 36:1035.
29. Chowdhury S, Izatt J. Biomed Opt Express. 2013; 4:1795. [PubMed: 24156044]
30. Kim M, Choi Y, Fangyen C, Sung Y, Dasari RR, Feld MS, Choi W. Opt Lett. 2011; 36:148. [PubMed: 21263482]
31. Shin S, Kim K, Yoon J, Park YK. Opt Lett. 2015; 40:5407. [PubMed: 26565886]
32. Schubert R, Vollmer A, Ketelhut S, Kemper B. Biomed Opt Express. 2014; 5:4213. [PubMed: 25574433]

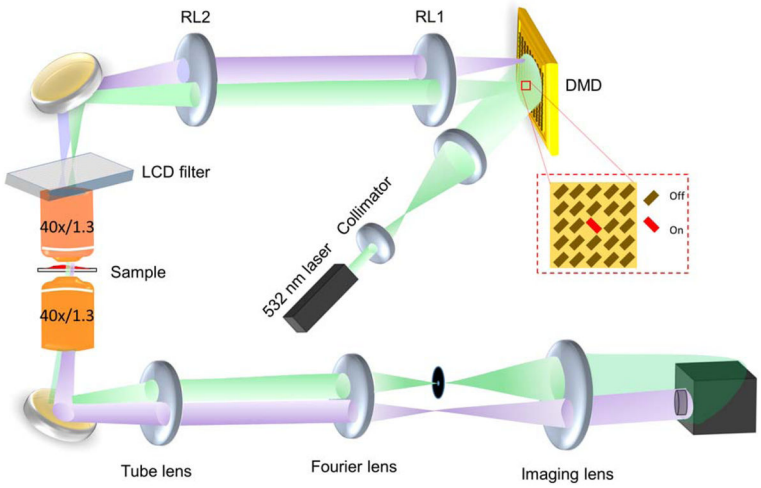

Fig. 1.

Schematic of the DMD-based common-path QPI system. An inset shows a magnified view of a DMD region consisting of different micromirrors that can be turned “on” and “off” individually. When one pixel is “on,” fraction of the laser beam from that pixel will be directed to the optical system and generate a plane wave illuminating the sample at a particular angle.

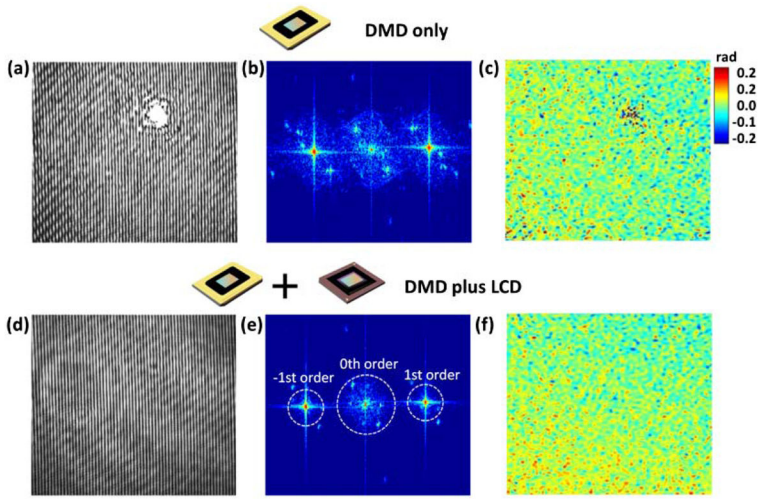

Fig. 2.

Enhanced interference contrast using the DMD-LCD combination. (a) Measured interferogram using the DMD only. (b) The modulus of the Fourier transform of (a) in log scale. (c) The corresponding phase image of (a). (d) Measured interferogram using the DMD-LCD combination. (e) The modulus of the Fourier transform of (d) in log scale. (f) The corresponding phase image of (d).

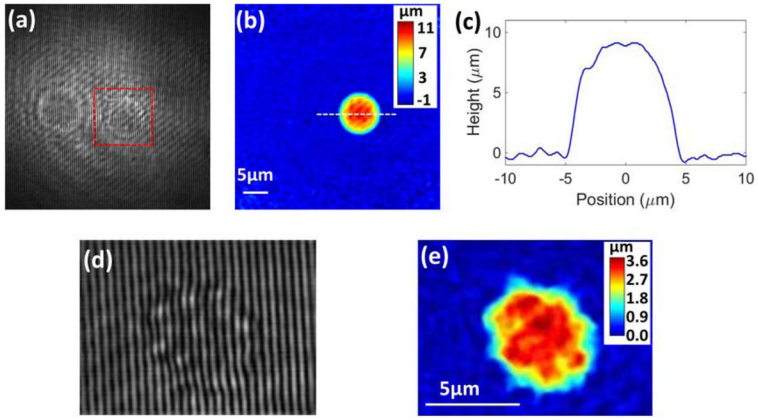

Fig. 3.

Quantitative phase imaging of a polystyrene bead and RBC. (a) An interferogram containing a 10-μm-diameter bead. (b) The height map of the bead. (c) The line profile across the center of the bead. (d) An interferogram of an echinocyte. (e) The height map of the echinocyte.

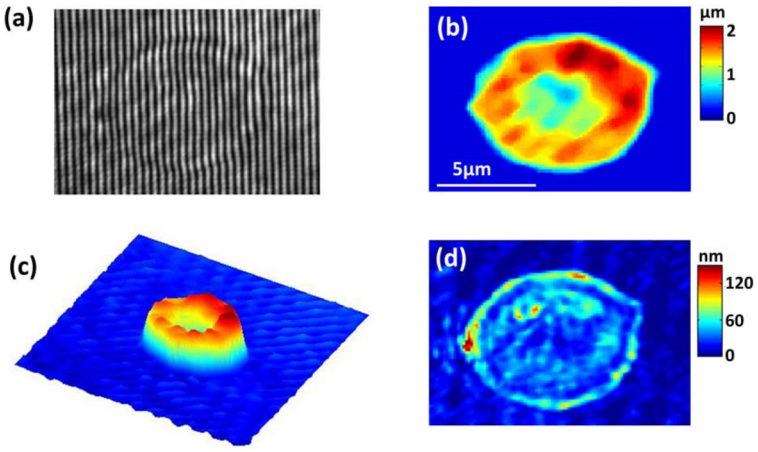

Fig. 4.

Quantifying the membrane fluctuations of a living RBC. (a) An interferogram containing a discocyte. (b) The height map of the discocyte. (c) A time-lapse showing the discocyte membrane fluctuations (see Visualization 1). (d) A standard deviation map of the membrane height fluctuation.

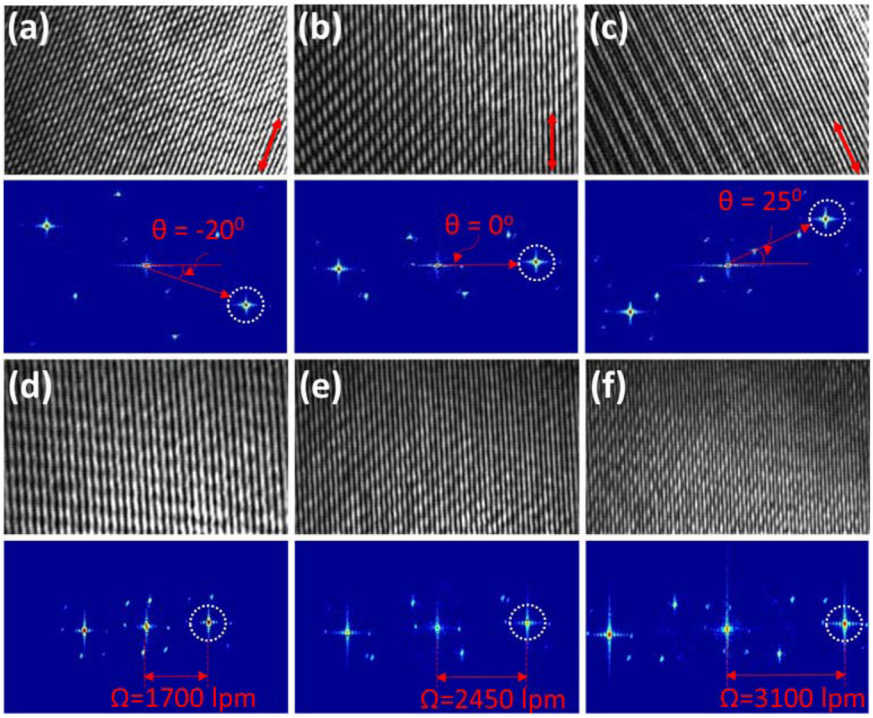

Fig. 5.

Orientation angle and period modulation of the interfero-gram fringe. (a)–(c) Interferogram fringe orientation at −20 deg, 0 deg, and 25 deg. (d)–(f) Interferogram fringe frequency of 1700 lpm, 2450 lpm, and 3100 lpm. lpm: lines per millimeter.